

Updating TMD parton densities in a proton within the Kimber-Martin-Ryskin approach

A.V. Kotikov¹, A.V. Lipatov²

February 27, 2025

¹*Joint Institute for Nuclear Research, 141980 Dubna, Moscow region, Russia*

²*Skobeltsyn Institute of Nuclear Physics, Lomonosov Moscow State University, 119991 Moscow, Russia*

Abstract

We present analytical expressions for the Transverse Momentum Dependent (TMD, or unintegrated) gluon and quark densities in a proton derived at leading order of QCD running coupling and valid at both small and large x . The calculations are performed using the Kimber-Martin-Ryskin/Watt-Martin-Ryskin prescription (in both differential and integral formulations) with different treatment of kinematical constraint, which reflects the angular and strong ordering conditions for parton emissions. As an input, analytical solution of QCD evolution equations for conventional (collinear) parton distributions is applied, where the valence and non-singlet quark parts obey the Gross-Llewellyn-Smith and Gottfried sum rules and momentum conservation for the singlet quark and gluon densities is taken into account. Several phenomenological parameters are extracted from combined fit to precision data on the proton structure function $F_2(x, Q^2)$ collected by the BCDMS, H1 and ZEUS Collaborations, comprising a total of 933 points from 5 data sets. Comparison with the numerical results obtained by other groups is presented and phenomenological application to the inclusive b -jet production at the LHC is given.

Keywords: QCD evolution, parton density functions, small- x physics, Kimber-Martin-Ryskin approach, High Energy Factorization

1 Introduction

It is well known that theoretical description of hadronic collisions at high energies which proceed with large momentum transfer and involve several hard scales can be achieved in the framework of High Energy Factorization [1] (or k_T -factorization [2]) approach of Quantum Chromodynamics (QCD). An essential point of this formalism is using the Transverse Momentum Dependent (TMD) parton (gluon and quark) distribution functions¹ in a proton and/or nuclei, $f_a(x, \mathbf{k}_T^2, \mu^2)$. These quantities depend on the fraction x of the colliding hadron longitudinal momentum carried by an interacting parton a , its two-dimensional transverse momentum \mathbf{k}_T^2 and hard scale μ^2 of the corresponding partonic scattering subprocess. The TMD parton densities encode nonperturbative information on hadron structure, including transverse momentum and polarization degrees of freedom and are under active investigation at present². In particular, their detailed knowledge is necessary for accurate theoretical predictions for cross sections of number of semi-inclusive and multiscale QCD processes studied currently at modern colliders (LHC, RHIC) and planned to be studied at future machines (FCC-he, EIC, EicC, NICA, CEPC etc).

In contrast with a great amount of our knowledge about the conventional (collinear) parton distribution functions (PDFs), $f_a(x, \mu^2)$, accumulated over past years, the TMD parton densities in a proton and especially nuclei are rather poorly known quantities still. In the asymptotical limit of high energies (or, equivalently, low x) the TMD gluon distributions must satisfy famous Balitsky-Fadin-Kuraev-Lipatov (BFKL) [9] evolution equation, where large logarithmic contributions to the production cross section proportional to $\alpha_s^n \ln^n s / \Lambda_{\text{QCD}}^2 \sim \alpha_s^n \ln^n 1/x$ are taken into account. Such terms are expected to be even more important in comparison with conventional Dokshitzer-Gribov-Lipatov-Altarelli-Parisi (DGLAP) [10] contributions, which are proportional to $\alpha_s^n \ln^n \mu^2 / \Lambda_{\text{QCD}}^2$. Also, the Catani-Ciafaloni-Fiorani-Marchesini (CCFM) equation [11], which additionally resums terms proportional to $\alpha_s^n \ln^n 1/(1-x)$ and BK [12] or JIMWLK equations [13–18], where non-linear effects are taken into account, can be used to describe the non-collinear (dependent on the transverse momentum) QCD evolution.

Other popular approaches to derive the TMD parton distributions are the so-called Kimber-Martin-Ryskin (KMR) [19] or Watt-Martin-Ryskin (WMR) [20] prescriptions, which are formalisms to construct the TMDs from well-known collinear PDFs. Note that the WMR approach is an extension and further development of early KMR ideas and explored currently at the next-to-leading order (NLO) [21]. The key assumption of the KMR/WMR formalism is that the dependence of parton distributions on the transverse momentum enters only at the last evolution step, so that the standard DGLAP scenario could be applied up to this step. Such prescription, where ordinary PDFs (as obtained numerically, for example, by the NNPDF [22], MHST [23], CTEQ-TEA [24,25] or IMP [26] groups) are employed as an input for the KMR/WMR procedure, is widely used in the phenomenological applications (see, for example, [27–32] and references therein).

In the present paper, the KMR/WMR formalism is employed for analytical calculations of the TMD parton densities in a proton valid at both small and large x . As a first step, our calculations are limited to leading order (LO) of the perturbation theory. The LO approximation is reasonable for processes, where the NLO corrections are still not known. Moreover, most of phenomenological applications of k_T -factorization

¹In the k_T -factorization literature, the TMD parton densities are also often referred as unintegrated parton distributions (uPDFs). Hereafter we will use first notation, TMDs.

²They are widely used also in the Collins-Soper-Sterman approach (or TMD factorization) [3–6], which is designed for semi-inclusive processes with a finite and non-zero ratio between the hard scale μ^2 and total energy s (see also reviews [7,8] for more information).

approach are currently performed at LO³. Our derivation is mainly based on the expressions [35] for conventional PDFs obtained (in the fixed-flavor-number scheme, FFNS) from the analytical solution of the DGLAP evolution equations. The expressions [35] rely on exact asymptotics at low and large values of x and contain subasymptotic terms fixed by the momentum conservation and, in the non-singlet and valence parts, by the Gross-Llewellyn-Smith and Gottfried sum rules, respectively. In contrast with the preliminary study [35], here we perform a rigorous fit to precision BCDMS, H1 and ZEUS experimental data [36–41] on the proton structure function $F_2(x, Q^2)$ to determine necessary phenomenological parameters involved into the formulas [35]. The data [36–41] cover extremely wide kinematical region, $2 \cdot 10^{-5} < x < 0.75$ and $1.2 < Q^2 < 30000 \text{ GeV}^2$. Then we derive analytical expressions for the proton TMDs with different treatment of kinematical constraint. This constraint is used in the KMR/WMR prescription and corresponds to the angular or strong ordering condition for parton emissions at the last evolution step. Finally, we test the obtained TMDs with beauty production in pp collisions at the LHC. Here we rely on our previous investigations [42, 43]. We calculate total and differential cross sections for b -jet and $b\bar{b}$ -dijet events and compare our predictions with available CMS [44, 45] and ATLAS [46] experimental data taken at $\sqrt{s} = 7 \text{ TeV}$.

Our present study is the continuation of previous investigations [47–49], where small- x asymptotics for the TMD parton densities in a proton and nuclei were considered. Moreover, it significantly improves our preliminary results [35], where some of phenomenological parameters of the analytical solution of the DGLAP evolution equations have been determined rather roughly. The main advantage of the developed approach is related with a quite compact analytical formulas for the TMD parton densities in a proton, which could be easily applied in further phenomenological studies and also could be extended to the nuclear distributions.

The outline of our paper is following. In Section 2 we describe our theoretical input. Here we list small- x and large- x asymptotics which are used to construct the PDFs in a whole kinematical region. Section 3 is devoted to determination of the TMD parton densities in the KMR/WMR framework, where all calculations are explained in detail. Section 4 presents our numerical results and discussions. Section 5 contains our conclusions.

2 The model

Here we shortly review small- x and large- x asymptotics of the conventional PDFs presented previously [35]. For the reader's convenience, we also list the basic formulas of the LO KMR/WMR approach itself.

2.1 Proton PDFs and structure function $F_2(x, Q^2)$

We start from some basic formulas. As it is known, the proton structure function $F_2(x, Q^2)$ at the LO of perturbative QCD expansion can be presented in the simple form (see, for example, [50, 51])

$$F_2(x, Q^2) = F_2^{\text{LT}}(x, Q^2) \left(1 + \frac{h(x)}{Q^2} \right), \quad (1)$$

³First attempts to include higher order corrections were done (see, for example, [33, 34] and references therein).

with the leading twist (LT) part

$$F_2^{\text{LT}}(x, Q^2) = \sum_i^{N_f} e_i^2 [f_{q_i}(x, Q^2) + f_{\bar{q}_i}(x, Q^2)], \quad (2)$$

where e_i is the fractional electric charge of quark q_i and $f_{q_i}(x, Q^2)$ and $f_{\bar{q}_i}(x, Q^2)$ are the quark and antiquark densities in a proton (multiplied by x), respectively. The magnitude $h(x)$ of the twist-four part is poorly known theoretically and usually can be represented in the form

$$h(x) = h_0 + \frac{h_1}{1-x}, \quad \text{or} \quad h(x) = \bar{h}x^{-\delta} + h_0 + \frac{h_1}{1-x} \quad (3)$$

with $\delta \sim 0.18 \div 0.2$ [50] and h_0 , h_1 and \bar{h} being free parameters.

Everywhere below we use the fixed-flavor-number-scheme⁴ (FFNS) with $N_f = 4$. In this scheme, where b and t quarks are separated out, we have

$$F_2^{\text{LT}}(x, Q^2) = \frac{5}{18} f_{SI}(x, Q^2) + \frac{1}{6} f_{NS}(x, Q^2). \quad (4)$$

In the formulas above the singlet part $f_{SI}(x, \mu^2)$ contains the valence (V) and sea (S) quark parts:

$$\begin{aligned} f_V(x, \mu^2) &= f_u^V(x, \mu^2) + f_d^V(x, \mu^2), \quad f_S(x, \mu^2) = \sum_{i=1}^{N_f} [f_{q_i}^S(x, \mu^2) + f_{\bar{q}_i}^S(x, \mu^2)], \\ f_{SI}(x, \mu^2) &= \sum_{i=1}^{N_f} [f_{q_i}(x, \mu^2) + f_{\bar{q}_i}(x, \mu^2)] = f_V(x, \mu^2) + f_S(x, \mu^2). \end{aligned} \quad (5)$$

The nonsinglet part $f_{NS}(x, \mu^2)$ contains difference between the up and down quarks:

$$f_{NS}(x, \mu^2) = \sum_{q=u,c} [f_q(x, \mu^2) + f_{\bar{q}}(x, \mu^2)] - \sum_{q=d,s} [f_q(x, \mu^2) + f_{\bar{q}}(x, \mu^2)]. \quad (6)$$

All these formulas above are very useful in accurate determination of phenomenological parameters of proton PDFs derived in our previous paper [35]. Note that approach [35] follows the idea [52] and consists of two basic steps. First of them is the analytical calculation of the asymptotics of solutions of the DGLAP equations for the parton densities at low and large values of Bjorken variable x . Second, to obtain the analytical expressions for PDFs over the full x range, one can combine these solutions and then interpolate between them (see also [53]).

2.2 Non-singlet and valence quark parts

The non-singlet and valence parts of quark distribution functions can be represented in the following form [35]:

$$f_i(x, \mu^2) = \left[A_i(s) x^{\lambda_i} (1-x) + \frac{B_i(s) x}{\Gamma(1 + \nu_i(s))} + D_i(s) x(1-x) \right] (1-x)^{\nu_i(s)}, \quad (7)$$

⁴The FFNS results with $N_f = 4$ can be obtained in the simplest way. Moreover, the results are usually very similar (see [51]) to ones obtained in the variable-flavor-number-scheme (VFNS). However, the application of the latter is more complicated. We plan to perform VFNS studies in our future investigations.

where $i = NS$ or V , $s = \ln [\alpha_s(Q_0^2)/\alpha_s(\mu^2)]$ and

$$A_i(s) = A_i(0)e^{-d(n_i)s}, \quad B_i(s) = B_i(0)e^{-ps}, \quad \nu_i(s) = \nu_i(0) + rs, \\ r = \frac{16}{3\beta_0}, \quad p = r(\gamma_E + \hat{c}), \quad \hat{c} = -\frac{3}{4}, \quad d(n) = \frac{\gamma_{NS}(n)}{2\beta_0}, \quad n_i = 1 - \lambda_i. \quad (8)$$

Here $\Gamma(z)$ is the Riemann's Γ -function, $\gamma_E \simeq 0.5772$ is the Euler's constant, $\beta_0 = 11 - (2/3)N_f$ is the LO QCD β -function and $\gamma_{NS}(n)$ is the LO non-singlet anomalous dimension. From the Regge calculus, $\lambda_{NS} \simeq \lambda_V \simeq 0.3 - 0.5$. For the simplicity, here we set $\lambda_{NS} = \lambda_V = 0.5$. Everywhere below, we apply "frozen" treatment of the QCD coupling in the infrared region (see, for example, [54, 55] and references therein), where $\alpha_s(\mu^2) \rightarrow \alpha_s(\mu^2 + M_\rho^2)$ with $M_\rho \sim 1$ GeV, that immediately leads to $s > 0$. Such treatment results in a good description of the data on proton structure function $F_2(x, Q^2)$ at low Q^2 [54].

As it was mentioned above, the expression (7) is constructed as the combination of the small- x part proportional to $A_i(s)$, large- x asymptotic proportional to $B_i(s)$ and additional term proportional to $D_i(s)$. The latter is subasymptotics in both these regions and fixed by the Gross-Llewellyn-Smith and Gottfried sum rules [35]:

$$D_i(s) = (2 + \nu_i(s)) \left[N_i - A_i(s) \frac{\Gamma(\lambda_i)\Gamma(2 + \nu_i(s))}{\Gamma(\lambda_i + 2 + \nu_i(s))} - \frac{B_i(s)}{\Gamma(2 + \nu_i(s))} \right], \quad (9)$$

where $N_V = 3$ and

$$N_{NS} = 1 + 2 \int_0^1 \frac{dx}{x} [f_{\bar{u}}(x, \mu^2) + f_{\bar{c}}(x, \mu^2) - f_{\bar{d}}(x, \mu^2) - f_{\bar{s}}(x, \mu^2)] \equiv I_G(\mu^2). \quad (10)$$

The μ^2 -dependence of $I_G(\mu^2)$ is very weak [56] and, therefore, can be safely neglected in our LO analysis. So, everywhere below we use $I_G(\mu^2) \equiv I_G = 0.705 \pm 0.078$ [57].

Free parameters $A_i(0)$, $B_i(0)$ and $\nu_i(0)$ involved in (7) and (8) can be determined, for example, from the direct comparison with appropriate numerical solutions [24] of the DGLAP equations or from experimental data (see below).

2.3 Singlet quark and gluon parts

The sea and gluon densities in a proton can be represented as combinations of " \pm " terms in the following form [35] (see also [58]):

$$f_i(x, \mu^2) = f_i^+(x, \mu^2) + f_i^-(x, \mu^2), \quad (11)$$

where $i = SI$ or g and

$$f_{SI}^-(x, \mu^2) = \tilde{f}_{SI}^-(x, \mu^2)(1-x)^{\nu^-(s)}, \quad f_{SI}^+(x, \mu^2) = \tilde{f}_{SI}^+(x, \mu^2)(1-x)^{\nu^+(s)+1}, \\ f_g^-(x, \mu^2) = \tilde{f}_g^-(x, \mu^2)(1-x)^{\nu^-(s)+1}, \quad f_g^+(x, \mu^2) = \tilde{f}_g^+(x, \mu^2)(1-x)^{\nu^+(s)}, \quad (12)$$

with

$$\tilde{f}_{SI}^+(x, \mu^2) = \frac{N_f}{9} \left[A_g + \frac{4}{9} A_q \right] \rho I_1(\sigma) e^{-\bar{d}^+ s} (1-x)^{m_q^+} + D^+(s) \sqrt{x} (1-x)^{n^+} - \\ - \frac{K^+}{\Gamma(2 + \nu^+(s))} \times \frac{B^+(s)x}{\hat{c} - \ln(1-x) + \Psi(2 + \nu^+(s))}, \quad (13)$$

$$\tilde{f}_{SI}^-(x, \mu^2) = A_q e^{-d^- s} (1-x)^{m_q^-} + \frac{B^-(s)x}{\Gamma(1+\nu^-(s))} + D^-(s) \sqrt{x} (1-x)^{n^-}, \quad (14)$$

$$\tilde{f}_g^+(x, \mu^2) = \left(A_g + \frac{4}{9} A_q \right) I_0(\sigma) e^{-\bar{d}^+ s} (1-x)^{m_g^+} + \frac{B^+(s)x}{\Gamma(1+\nu^+(s))}, \quad (15)$$

$$\begin{aligned} \tilde{f}_g^-(x, \mu^2) = & -\frac{4}{9} A_q e^{-d^- s} (1-x)^{m_g^-} + \\ & + \frac{K^-}{\Gamma(2+\nu^-(s))} \times \frac{B^-(s)x}{\hat{c} - \ln(1-x) + \Psi(2+\nu^-(s))}. \end{aligned} \quad (16)$$

Here $\Psi(z)$ is the Riemann's Ψ -function, $I_0(z)$ and $I_1(z)$ are the modified Bessel functions and

$$\begin{aligned} \nu^\pm(s) &= \nu^\pm(0) + r^\pm s, \quad B^\pm(s) = B^\pm(0) e^{-p^\pm s}, \quad p^\pm = r^\pm(\gamma_E + \hat{c}^\pm), \\ r^+ &= \frac{12}{\beta_0}, \quad r^- = \frac{16}{3\beta_0}, \quad \hat{c}^+ = -\frac{\beta_0}{12}, \quad \hat{c}^- = -\frac{3}{4}, \quad K^+ = \frac{3N_f}{10}, \quad K^- = \frac{2}{5}, \\ \rho &= \frac{\sigma}{2\ln(1/x)}, \quad \sigma = 2\sqrt{|\hat{d}^+| s \ln \frac{1}{x}}, \\ \hat{d}^+ &= -\frac{12}{\beta_0}, \quad \bar{d}^+ = 1 + \frac{20N_f}{27\beta_0}, \quad d^- = \frac{16N_f}{27\beta_0} \end{aligned} \quad (17)$$

with $n^+ \sim n^-$ being free parameters. The small- x PDFs asymptotics seen in (13) — (2.3) were obtained at LO [55, 59–61] in the so-called generalized doubled asymptotic scaling (DAS) approximation [59, 60, 62]. In this approximation, flat initial conditions for proton PDFs, $f_g(x, Q_0^2) = A_g$ and $f_S(x, Q_0^2) = A_q$, can be used⁵. In the numerical analysis below we set $m_q^- = m_g^+ = 2$, $m_q^+ = m_g^- = 8$. In this case, small- x asymptotics above are suppressed at large x compared to subasymptotic terms proportional to $D^\pm(s)$. Moreover, these small- x asymptotics contain the same powers of $(1-x)$ factor for both quarks and gluons.

The expressions for $D^\pm(s)$ could be derived from the momentum conservation law [35]:

$$\begin{aligned} D^+(s) &= -\frac{\Gamma(7/2 + n^+ + \nu^+(s))}{\Gamma(3/2)\Gamma(2 + n^+ + \nu^+(s))} [G_{SI}^+(s) + \bar{G}_g^+(s)], \\ D^-(s) &= \frac{\Gamma(5/2 + n^- + \nu^-(s))}{\Gamma(3/2)\Gamma(1 + n^- + \nu^-(s))} [1 - G_g^-(s) - \bar{G}_{SI}^-(s)], \end{aligned} \quad (18)$$

where

$$\begin{aligned} G_{SI}^+(s) &= \frac{N_f}{9} \left[A_g + \frac{4}{9} A_q \right] \Phi_1(1 + m_q^+ + \nu^+(s)) e^{-\bar{d}^+ s} - \\ & - \frac{K^+ B^+(s)}{\Gamma(4 + \nu^+(s))(\Psi(4 + \nu^+(s)) + \hat{c})}, \end{aligned} \quad (19)$$

$$\bar{G}_g^+(s) = \left[A_g + \frac{4}{9} A_q \right] \Phi_0(m_g^+ + \nu^+(s)) e^{-\bar{d}^+ s} + \frac{B^+(s)}{\Gamma(3 + \nu^+(s))}, \quad (20)$$

$$G_g^-(s) = -\frac{4A_q}{9(2 + \nu^-(s) + m_g^-)} e^{-d^- s} + \frac{K^- B^-(s)}{\Gamma(4 + \nu^-(s))(\Psi(4 + \nu^-(s)) + \hat{c})}, \quad (21)$$

$$\bar{G}_{SI}^-(s) = \frac{A_q}{1 + \nu^-(s) + m_q^-} e^{-d^- s} + \frac{B^-(s)}{\Gamma(3 + \nu^-(s))}, \quad (22)$$

⁵The NLO analysis has been done [59, 60].

and

$$\Phi_0(\nu) = \int_0^1 dx I_0(\sigma)(1-x)^{\nu(s)}, \quad \Phi_1(\nu) = \int_0^1 dx \rho I_1(\sigma)(1-x)^{\nu(s)}. \quad (23)$$

At large ν one can use the following approximation (see [35] for more details):

$$\Phi_0(\nu) \simeq \frac{1}{1+\nu} I_0 \left(2\sqrt{|\hat{d}_+|s (\ln(1+\nu) + \gamma_E)} \right), \quad (24)$$

$$\Phi_1(\nu) \simeq \frac{1}{1+\nu} \left(\sqrt{\frac{|\hat{d}_+|s}{\ln(1+\nu) + \gamma_E}} \right) I_1 \left(2\sqrt{|\hat{d}_+|s (\ln(1+\nu) + \gamma_E)} \right). \quad (25)$$

The exact values of all free parameters A_g , A_q , $B^\pm(0)$, $\nu^\pm(0)$ and n^\pm could be taken from the fit to experimental data.

2.4 LO KMR/WMR approach

As it was mentioned above, the KMR/WMR approach is a formalism to construct the TMD parton distributions from well-known ordinary PDFs. The key assumption is that the transverse momentum dependence of the parton densities enters only at the last evolution step. This procedure is believed to take into account effectively the major part of next-to-leading logarithmic (NLL) terms $\alpha_s(\alpha_s \ln \mu^2 / \Lambda_{\text{QCD}}^2)^{n-1}$ compared to the leading logarithmic approximation (LLA), where terms proportional to $\alpha_s^n \ln^n \mu^2 / \Lambda_{\text{QCD}}^2$ are taken into account.

There are known differential (d) and integral (i) definitions of the KMR/WMR prescription. According to these definitions, the TMD parton densities in a proton can be calculated as [19]

$$f_a^{(d)}(x, \mathbf{k}_T^2, \mu^2) = \frac{\partial}{\partial \ln \mathbf{k}_T^2} [T_a(\mathbf{k}_T^2, \mu^2) f_a(x, \mathbf{k}_T^2)], \quad (26)$$

$$f_a^{(i)}(x, \mathbf{k}_T^2, \mu^2) = 2a_s(\mathbf{k}_T^2) T_a(\mathbf{k}_T^2, \mu^2) \sum_b \int_x^{1-\Delta} dz P_{ab}(z) f_b\left(\frac{x}{z}, \mathbf{k}_T^2\right), \quad (27)$$

where $a = q$ or g , $a_s(\mu^2) = \alpha_s(\mu^2)/4\pi$, $T_a(\mathbf{k}_T^2, \mu^2)$ are the Sudakov form factors and $f_a(x, \mu^2) = xD_a(x, \mu^2)$ are the standard PDFs obeying the DGLAP equations:

$$\begin{aligned} \frac{\partial D_a(x, \mu^2)}{\partial \ln \mu^2} &= 2a_s(\mu^2) \sum_b \int_x^{1-\Delta} \frac{dz}{z} P_{ab}(z, \mu^2) D_b\left(\frac{x}{z}, \mu^2\right) - \\ &- D_a(x, \mu^2) \sum_b \int_0^{1-\Delta} dz z P_{ba}(z, \mu^2). \end{aligned} \quad (28)$$

Here Δ is some cutoff parameter (see below) and $P_{ab}(z)$ are the unregulated LO DGLAP splitting functions:

$$\begin{aligned} P_{qq}(z) &= C_F \left[\frac{1+z^2}{(1-z)_+} + \frac{3}{2} \delta(1-z) \right], \quad P_{qg}(z) = N_f \left[z^2 + (1-z)^2 \right], \\ P_{gq}(z) &= C_F \left[\frac{1+(1-z)^2}{z} \right], \\ P_{gg}(z) &= 2C_A \left[\frac{z}{(1-z)_+} + \frac{1-z}{z} + z(1-z) + \frac{\beta_0}{12} \delta(1-z) \right]. \end{aligned} \quad (29)$$

The quark and gluon Sudakov form factors $T_a(\mathbf{k}_T^2, \mu^2)$ give the probability of evolving from a scale \mathbf{k}_T^2 to a scale μ^2 without parton emission:

$$\ln T_a(\mathbf{k}_T^2, \mu^2) = -2 \int_{\mathbf{k}_T^2}^{\mu^2} \frac{d\mathbf{p}_T^2}{\mathbf{p}_T^2} a_s(\mathbf{p}_T^2) \sum_b \int_0^{1-\Delta} dz z P_{ba}(z). \quad (30)$$

As it is often done, we set $T_a(\mathbf{k}_T^2, \mu^2) = 1$ at $\mathbf{k}_T^2 > \mu^2$.

Several important remarks are in order. First, both integrals appearing in (28), which describe real and virtual parton emissions, are divergent at $\Delta = 0$ due to the singular splitting functions $P_{qq}(z)$ and $P_{gg}(z)$ at $z = 1$. However, these singularities, which are due to soft radiation, cancel out when the two terms are combined through the "+" prescription. In contrast, if the upper integration limits in (28) and (30) are restricted by some $\Delta > 0$, then δ -functions in (29) give no contributions. Moreover, the "+" prescription is not needed: $(1-z)_+^{-1} \rightarrow (1-z)^{-1}$. In this case, the positive real emissions are separated from negative virtual ones, that could results in some ambiguities in the KMR/WMR formalism (see, for example, discussions [63–66]). So, the differential and integral KMR/WMR definitions are not equivalent if ordinary PDFs are used in (26) and (27). In particular, the difference between two these definitions occur at large transverse momenta. It was shown [63] that (26) and (27) become mathematically equivalent if special cutoff Δ -dependent PDFs are employed instead of standard PDFs (as obtained from the DGLAP equations at $\Delta = 0$ and global fits to data). Nevertheless, the TMD parton densities derived from the integral definition (27) are practically the same, regardless on the choice of the ordinary or cutoff dependent PDFs in the calculations [63]. Thus, this definition seems to be more preferable in the phenomenological applications. Concerning the cutoff parameter Δ , usually it has one of two basic physically motivated forms:

$$\Delta_1 = \frac{|\mathbf{k}_T|}{\mu}, \quad \Delta_2 = \frac{|\mathbf{k}_T|}{|\mathbf{k}_T| + \mu}, \quad (31)$$

that reflects the strong ordering (SO) or angular ordering (AO) conditions for parton emissions at the last evolution step⁶ to regulate the soft gluon singularities (see [19] for more information). It is important that parton distributions $f_a(x, \mathbf{k}_T^2, \mu^2)$ extend into the $\mathbf{k}_T^2 > \mu^2$ region in the case of angular ordering and vanish at large \mathbf{k}_T^2 in the case of strong ordering condition.

Another point is related to the treatment of low \mathbf{k}_T^2 region. In fact, both the differential and integral definitions of the KMR/WMR approach are only correct at $\mathbf{k}_T^2 > \mu_0^2$, where $\mu_0^2 \sim 1 \text{ GeV}^2$ is the minimum scale where perturbative QCD is still applicable. At small \mathbf{k}_T^2 special model assumptions are necessary. Usually, such assumptions are connected with the normalization condition

$$f_a(x, \mu^2) = \int_0^{\mu_{\max}^2} f_a(x, \mathbf{k}_T^2, \mu^2) d\mathbf{k}_T^2, \quad (32)$$

where μ_{\max}^2 is taken to be equal to μ^2 (see, for example, [19, 63]) or even infinity [66]. The rather arbitrary shape of $f_a(x, \mathbf{k}_T^2, \mu^2)$ at low $\mathbf{k}_T^2 < \mu_0^2$ is often chosen, such as flat or Gaussian-like. However, in our consideration, where "frozen" treatment of the QCD coupling in the infrared region is applied, the TMDs are well defined in the whole \mathbf{k}_T^2

⁶The strong ordering in transverse momentum within the DGLAP equations automatically ensures angular ordering.

range. Thus, we do not use the normalization condition (32). Moreover, in our opinion, any relations between the TMDs and collinear PDFs can only be approximate since these quantities are essentially different objects where essentially different large logarithmic terms appearing in the perturbative QCD expansion are resummed.

3 Analytic results

The analytical expressions for conventional PDFs collected above could be used as an input for the KMR/WMR procedure, giving us the possibility to derive the analytical expressions for the TMD parton densities in a proton.

3.1 Differential definition

Now we calculate the TMD parton densities according to (26) without derivatives. Derivation of the $T_a(\mu^2, k^2)$ and conventional PDFs are as follows

$$\frac{\partial T_a(\mathbf{k}_T^2, \mu^2)}{\partial \ln \mathbf{k}_T^2} = d_a \beta_0 a_s(\mathbf{k}_T^2) R_a(\Delta), \quad (33)$$

$$\frac{\partial f_a(x, \mathbf{k}_T^2)}{\partial \ln \mathbf{k}_T^2} \approx -\beta_0 a_s(\mathbf{k}_T^2) \times \quad (34)$$

$$\times \left[\left(\frac{\hat{d}^+}{\rho_a} + \bar{d}^+ - r^+ \ln(1-x) \right) f_a^+(x, \mathbf{k}_T^2) + (d^- - r^- \ln(1-x)) f_a^-(x, \mathbf{k}_T^2) \right], \quad (35)$$

where

$$\begin{aligned} R_q(\Delta) &= \ln \left(\frac{1}{\Delta} \right) - \frac{3}{4}(1-\Delta)^2, \\ R_g(\Delta) &= \ln \left(\frac{1}{\Delta} \right) - \left(1 - \frac{\varphi}{4} \right) (1-\Delta)^2 + \frac{1-\varphi}{12} (1-\Delta)^3 (1+3\Delta), \\ d_a &= \frac{4C_a}{\beta_0}, \quad \hat{d}^+ = -|\hat{d}^+|, \quad \varphi = N_f/C_A, \quad C_q = C_F, \quad C_g = C_A, \\ \frac{1}{\rho_g} &= \frac{1}{\rho} \frac{I_1(\sigma)}{I_0(\sigma)}, \quad \frac{1}{\rho_q} = \frac{1}{\rho} \frac{I_0(\sigma)}{I_1(\sigma)}. \end{aligned} \quad (36)$$

We note that the result (35) is a simple extension of the one [?] to the whole x range. The extension contains the additional terms $\sim \ln(1-x)$. Nevertheless, we checked that (35) approximates with good accuracy the $\ln \mathbf{k}_T^2$ -derivative of the exact results (11) — (15). So, the final formula for the TMD parton densities reads

$$\begin{aligned} f_a^{(d)}(x, \mathbf{k}_T^2, \mu^2) &\approx \beta_0 a_s(\mathbf{k}_T^2) T_a(\mathbf{k}_T^2, \mu^2) \times \left(d_a R_a(\Delta) f_a(x, \mathbf{k}_T^2) - \right. \\ &\left. - \left[\left(\frac{\hat{d}_+}{\rho_a} + \bar{d}_+ - r^+ \ln(1-x) \right) f_a^+(x, \mathbf{k}_T^2) + (d^- - r^- \ln(1-x)) f_a^-(x, \mathbf{k}_T^2) \right] \right). \end{aligned} \quad (37)$$

The expressions for conventional PDFs are listed in the Sections 2.2 and 2.3. Since the value of \hat{d}_+ is negative and factor \hat{d}_+/ρ_a is large at small x , the TMD parton densities $f_a^{(d)}(x, \mathbf{k}_T^2, \mu^2)$ are positive. With increasing x , the results for the latter can be negative.

3.2 Integral definition

The corresponding results for TMDs in the integral formulation (27) are a bit more complicated. So, as it was done earlier [35], here we limit ourselves by an approximation. Similar to (11), we represent sea and gluon densities as combinations of "±" terms:

$$f_a^{(i)}(x, \mathbf{k}_T^2, \mu^2) = f_a^{(i),+}(x, \mathbf{k}_T^2, \mu^2) + f_a^{(i),-}(x, \mathbf{k}_T^2, \mu^2), \quad (38)$$

where $a = SI$ or g and

$$\begin{aligned} f_{SI}^{(i),-}(x, \mathbf{k}_T^2, \mu^2) &= \tilde{f}_{SI}^{(i),-}(x, \mathbf{k}_T^2, \mu^2)(1-x)^{\nu^-(s)}, \\ f_{SI}^{(i),+}(x, \mathbf{k}_T^2, \mu^2) &= \tilde{f}_{SI}^{(i),+}(x, \mathbf{k}_T^2, \mu^2)(1-x)^{\nu^+(s)+1}, \\ f_g^{(i),+}(x, \mathbf{k}_T^2, \mu^2) &= \tilde{f}_g^{(i),+}(x, \mathbf{k}_T^2, \mu^2)(1-x)^{\nu^+(s)}, \\ f_g^{(i),-}(x, \mathbf{k}_T^2, \mu^2) &= \tilde{f}_g^{(i),-}(x, \mathbf{k}_T^2, \mu^2)(1-x)^{\nu^-(s)+1}. \end{aligned} \quad (39)$$

After some algebra we have

$$\tilde{f}_g^{(i),\pm}(x, \mathbf{k}_T^2, \mu^2) = 4C_g a_s(\mathbf{k}_T^2) T_g(\mathbf{k}_T^2, \mu^2) \times \left[D_g^\pm(x, \Delta) + \tilde{D}_g^\pm(\Delta) \right] \tilde{f}_g^\pm\left(\frac{x}{1-\Delta}, \mathbf{k}_T^2\right), \quad (40)$$

$$\begin{aligned} \tilde{f}_q^{(i),\pm}(x, \mathbf{k}_T^2, \mu^2) &= 4C_q a_s(\mathbf{k}_T^2) T_q(\mathbf{k}_T^2, \mu^2) \times \\ &\left[D_q^\pm(x, \Delta) \tilde{f}_q^\pm\left(\frac{x}{1-\Delta}, \mathbf{k}_T^2\right) + \overline{D}_q(\Delta) \tilde{f}_g^\pm\left(\frac{x}{1-\Delta}, \mathbf{k}_T^2\right) \right], \end{aligned} \quad (41)$$

where

$$\begin{aligned} D_g^\pm(x, \Delta) &= \ln\left(\frac{1-x}{\Delta}\right) - 2(1-\Delta) + \frac{(1-\Delta)^2}{2} - \frac{(1-\Delta)^3}{3} - xS_1(\nu_\pm), \\ D_q^\pm(x, \Delta) &= \ln\left(\frac{1-x}{\Delta}\right) - \frac{(1-\Delta)}{4}(3-\Delta) - xS_1(\nu_\pm), \\ \tilde{D}_g^+ &= \frac{1}{\bar{\rho}_g} + \frac{4N_f}{81}, \quad \tilde{D}_g^- = \frac{9(1-\Delta)}{8}(3+\Delta), \quad \overline{D}_q = N_f \frac{1-\Delta}{18} (2\Delta^2 - \Delta + 3), \\ \bar{\sigma} &= \sigma\left(x \rightarrow \frac{x}{1-\Delta}\right), \quad \bar{\rho}_a = \rho_a\left(x \rightarrow \frac{x}{1-\Delta}\right), \end{aligned} \quad (42)$$

and $S_1(\nu) = \Psi(\nu+1) - \Psi(1)$.

We see that expressions (38) — (42) are rather simple extension of the ones [47] to the whole x range. Below we will demonstrate that these results are in good agreement with the exact numerical evaluations of $f_a^{(i)}(x, \mathbf{k}_T^2, \mu^2)$ based on (27) and (11) — (15).

4 Numerical results

We are now in position to present our numerical results. We start from the determination of phenomenological parameters involved into the derived analytical expressions for conventional PDFs as well as TMD parton densities in a proton. Then we test the latter with inclusive heavy jet production at the LHC conditions.

4.1 Determination of phenomenological parameters

There are several parameters in the analytical expressions for conventional PDFs in a proton which are not predicted by the theory. Some of them, namely, $A_V(0)$, $A_{NS}(0)$,

A_q	A_g	$A_V(0)$	$B_V(0)$	$A_{NS}(0)$	$B_{NS}(0)$
0.75 ± 0.02	1.13 ± 0.01	2.82 ± 0.01	$(1.06 \pm 0.05) \cdot 10^3$	0.279 ± 0.006	$(1.19 \pm 0.04) \cdot 10^2$
$B^+(0)$	$B^-(0)$	$\nu_V(0)$	$\nu_{NS}(0)$	$\nu^-(0)$	n^-
$(6.2 \pm 0.5) \cdot 10^1$	$(2.27 \pm 0.10) \cdot 10^2$	4.05 ± 0.02	3.23 ± 0.01	3.54 ± 0.02	4.66 ± 0.05

Table 1: The fitted values of various phenomenological parameters involved in our analytical expressions for PDFs and TMD parton densities in a proton.

$B_V(0)$, $B_{NS}(0)$, $\nu_V(0)$ and $\nu_{NS}(0)$, essential in the large- x region, we determine from the direct comparison with the numerical solutions of the DGLAP equations at the starting scale Q_0^2 . Here we employ the CT'14 (LO) parametrizations [24] obtained by the CTEQ-TEA group with $N_f = 4$, that fully corresponds our setup. The remaining parameters we determine by fitting the precise data on proton structure function $F_2(x, Q^2)$ taken by the BCDMS [36], H1 [37–40] and ZEUS [40, 41] Collaborations. These data cover extremely wide region of x and Q^2 , namely, $2 \cdot 10^{-5} < x < 0.75$ and $1.2 < Q^2 < 30000 \text{ GeV}^2$, thus providing us the possibility to extract all necessary parameters simultaneously. Note that we included into the fit procedure low- Q^2 data, where the higher-twist corrections could play a role. Such corrections are taken into account according to general expressions (1) — (3). Next, we set $n^+ \sim n^-$, $\nu^+(0) \sim \nu^-(0)$ and keep in mind that the QCD evolution will result in $\nu^+(s) > \nu^-(s)$ for $s > 0$. Our fit is based on the LO formulas (4) — (6), where we apply $Q_0^2 = 0.43 \text{ GeV}^2$, as it was done earlier [35, 58]. We use world averaged $\alpha_s(M_Z^2) = 0.1180$ [67] with $\Lambda_{\text{QCD}}^{(4)} = 118 \text{ MeV}$.

The results of our fit, comprising a total of 933 points from 5 data sets [36–41], are collected in Table 1. A perfect goodness, $\chi^2/d.o.f. = 1.408$, is achieved⁷. The experimental data involved into the fit procedures are compared with our predictions in Fig. 1, where shaded bands represent the fits uncertainties summed in quadratures. One can see that good agreement is obtained in a wide range of x and Q^2 .

We note that newly fitted values of A_q and A_g differ from the previous results [58]. The main source of this difference is that the small- x PDF asymptotics have been used in the analysis [58] and experimental data on proton structure function $F_2(x, Q^2)$ were considered at low x and not very high Q^2 only. In contrast, here we extended the consideration into whole region of x and Q^2 and take into account all the available data sets. Thus, in this point our analysis significantly improves the previous consideration [35, 58].

Some of the derived PDFs are shown in Fig. 2 as functions of x for several scales μ^2 , namely, $\mu^2 = 1, 10, 100$ and 1000 GeV^2 . Additionally, we show here the comparison between our predictions and corresponding FFNS results obtained by the CTEQ-TEA Collaboration [24] at $N_f = 4$ and VFNS predictions of the NNPDF4.0 [22], MSHT'2020 [23] and IMP [26] groups. One can see that, in fact, up to now the sizeable discrepancy between the different PDFs could be seen, especially at low $\mu^2 \sim 1 \text{ GeV}^2$. Nevertheless, at moderate and higher μ^2 we find a reasonable agreement between our analytical results and relevant numerical analyses. In particular, our fit and VFNS predictions from IMP group are very close to each other.

In Fig. 3 we show the TMD gluon densities in a proton calculated according to (37) and

⁷We have obtained also $h_0 = -0.65 \pm 0.14$, $h_1 = 0.44 \pm 0.13$ and $\bar{h} = 0.035 \pm 0.008$.

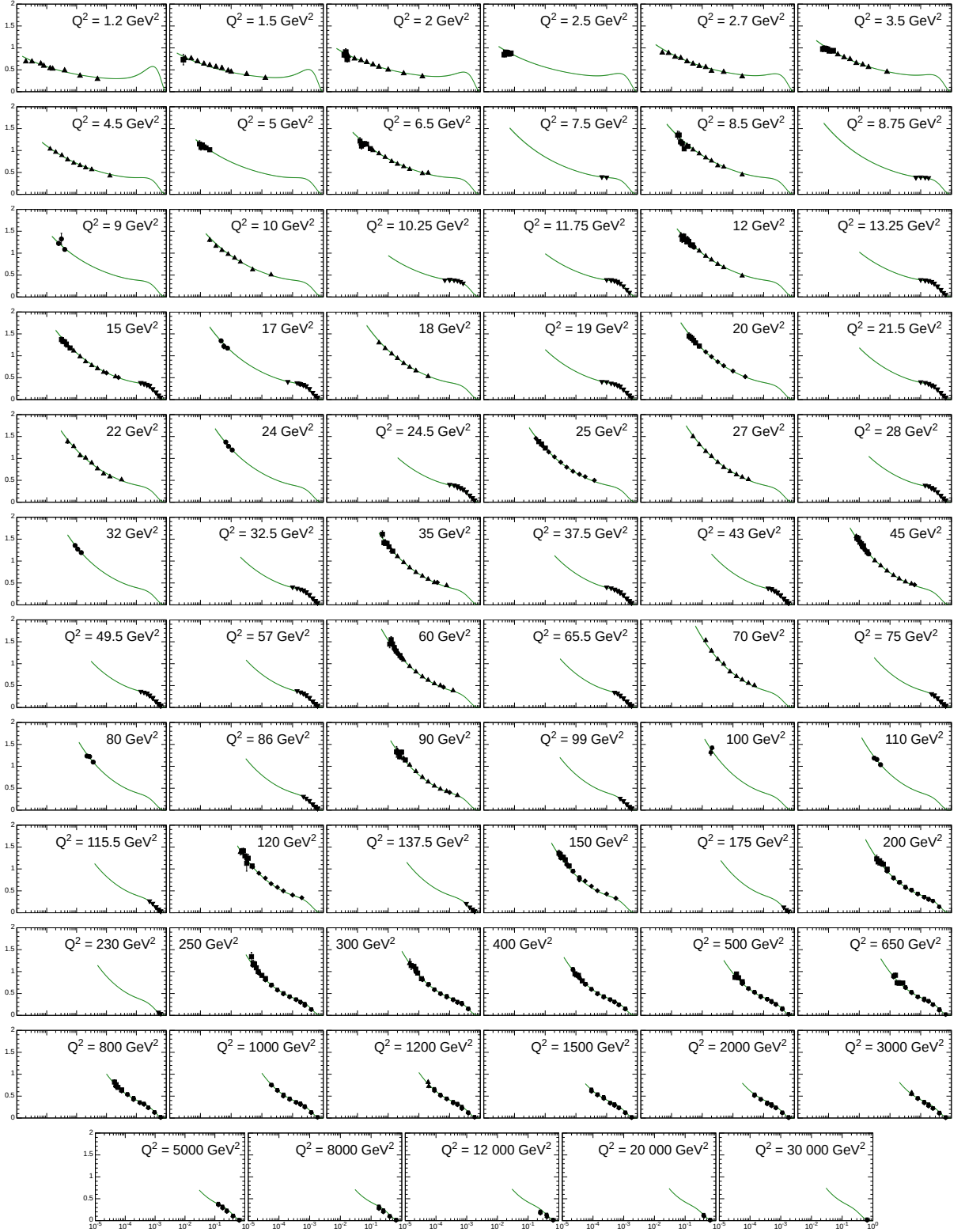


Figure 1: Proton structure function $F_2(x, Q^2)$ as a function of x for different Q^2 . The experimental data from BCDMS [36], H1 [37–40] and ZEUS [40, 41] Collaborations are compared with our fits.

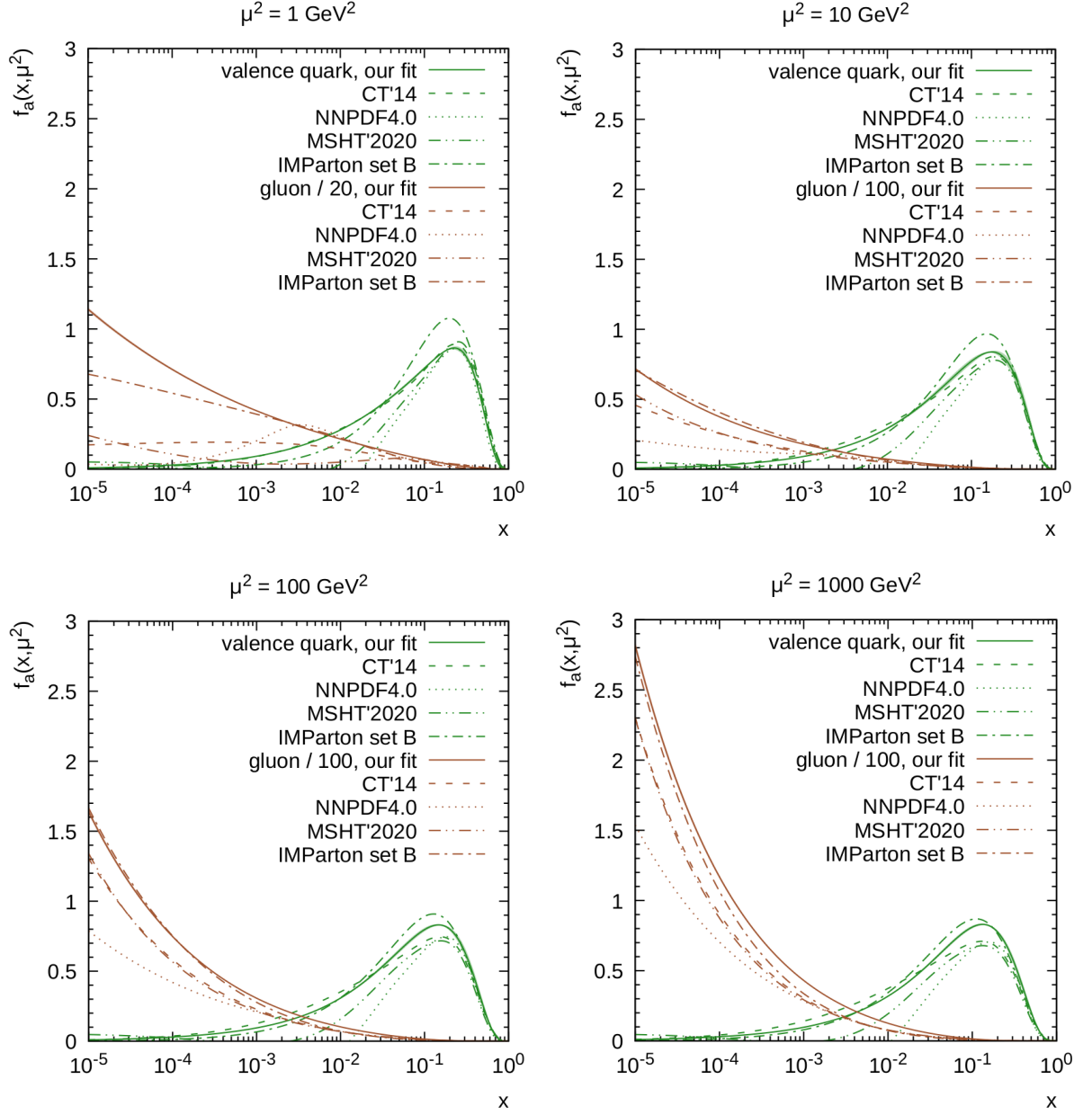


Figure 2: Proton PDFs calculated as function of x for different values of μ^2 . For comparison we show here the results of numerical solutions of the DGLAP equations performed by the CTEQ-TEA [24], NNPDF4.0 [22], MSHT'2020 [23] and IMP [26] groups.

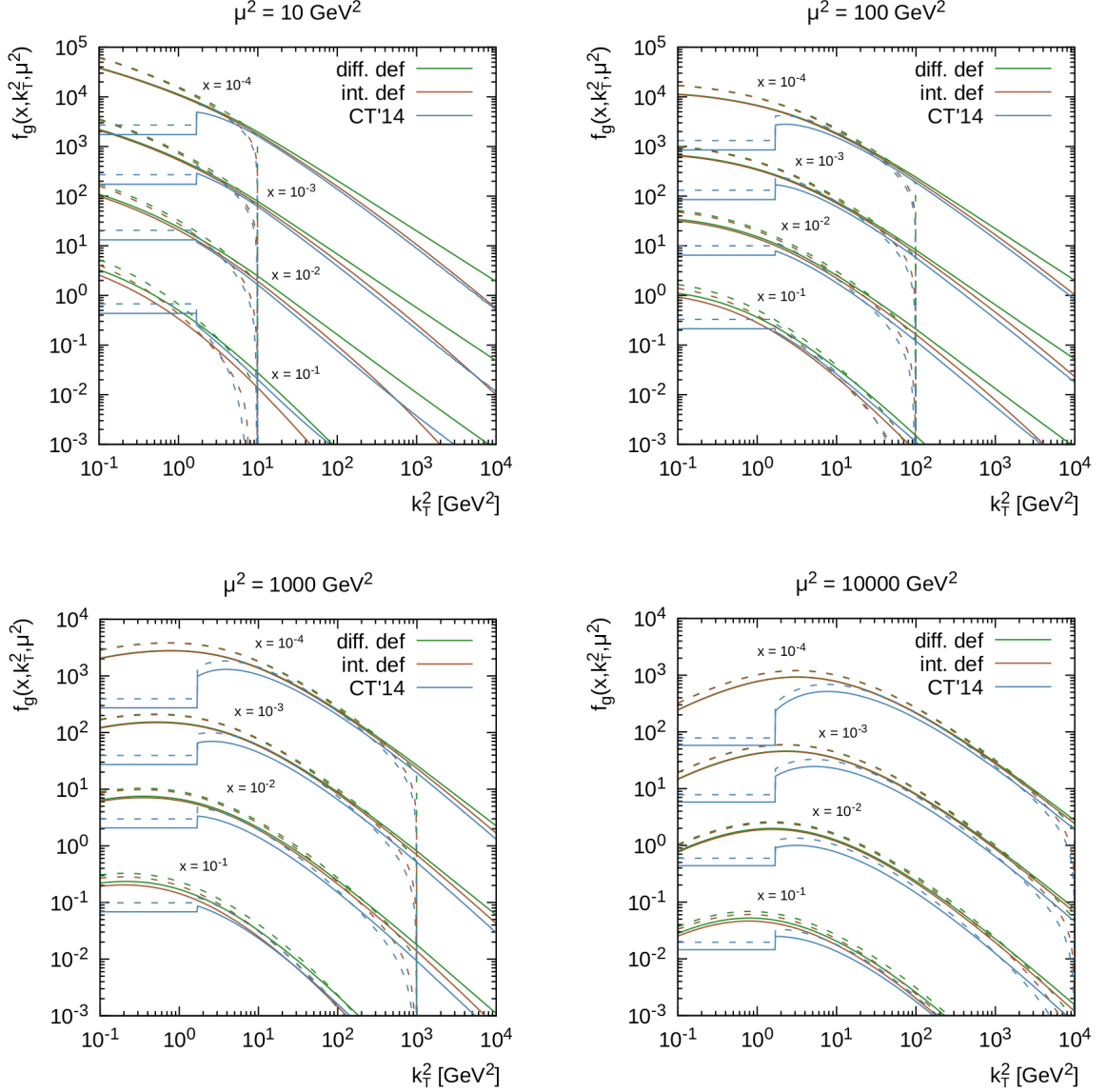


Figure 3: TMD gluon densities in a proton calculated as functions of \mathbf{k}_T^2 for different x and μ^2 using the angular ordering (solid curves) and strong ordering (dashed curves) conditions. Both the differential and integral KMR/WMR definitions have been applied for $N_f = 4$. For comparison we show corresponding results obtained numerically employing (27), where conventional PDFs from CT'14 set [24] have been used as an input.

(38) — (40) with different treatment of the angular ordering condition (31) as functions of transverse momentum \mathbf{k}_T^2 for several values of x and scale μ^2 . The solid and dashed curves correspond to the results obtained with the angular and strong ordering conditions, respectively. One can see that the differential and integral definitions of the KMR/WMR procedure lead to very close predictions at small x and low and moderate transverse momenta \mathbf{k}_T^2 , whereas some differences between them occur at large x and/or large \mathbf{k}_T^2 . It fully coincides with the observations [63], where the necessity of using the cutoff Δ dependent PDFs in the case of differential KMR/WMR definition was pointed out (see also discussions [65, 66]). Additionally, we plot here the TMD gluon densities obtained numerically employing the general integral KMR/WMR definition formula (27), where the conventional PDFs from CT'14 set [24] have been used as an input and popular normalization condition (32) with $\mu_{\text{max}}^2 = \mu^2$ and $Q_0 = 1.3$ GeV was applied. We find a notable agreement between these results and our corresponding predictions derived according to analytical expressions (38) — (40) at $\mathbf{k}_T^2 > Q_0^2$. Note that the flat behavior of former at $\mathbf{k}_T^2 < Q_0^2$ is due to commonly used assumptions in low \mathbf{k}_T^2 region. Finally, we demonstrate here again that the strong ordering condition leads to a steep drop of the gluon densities beyond the hard scale μ^2 . It contrasts with the angular ordering, where the gluon transverse momentum is allowed to be larger than μ^2 (see [19]).

4.2 Testing the TMDs: beauty production in pp collisions

Now we test the obtained analytical expressions (37) and (38) — (40) with beauty production in pp collisions at the LHC. These processes are promising for such study since they are known to be strongly sensitive to the gluon content of the proton⁸.

Our calculations are performed in the FFNS scheme with taking into account TMD gluon dynamics in a proton and strongly based on the previous considerations [42, 43]. In this approach, the main contribution to the heavy flavor production cross section comes from the off-shell gluon-gluon fusion subprocess $g^*(k_1) + g^*(k_2) \rightarrow Q(p_1) + \bar{Q}(p_2)$, where Q denotes outgoing beauty quark and four-momenta of all the particles are indicated in parentheses. The contribution from the quark-antiquark annihilation is of almost no importance because of comparatively low quark densities. According to the high energy factorization prescription [1, 2], corresponding production cross section can be written as a convolution of the TMD gluon densities and off-shell (depending on the transverse momenta of the incoming off-mass shell gluons) hard scattering amplitudes. The latter has been calculated a long time ago (see, for example, [1, 2, 42]). The detailed description of the calculation steps (including the evaluation of the off-shell gluon-gluon amplitudes) can be found [42]. We only specify here the essential numerical parameters. So, following [67], we set the beauty quark mass $m_b = 4.75$ GeV. Then, as it is often done, we choose the default renormalization and factorization scales μ_R and μ_F to be equal to the leading heavy jet transverse momentum. The calculations were performed using Monte-Carlo event generator PEGASUS⁹ [68].

The experimental data for beauty production in pp collisions at the LHC come from both CMS and ATLAS Collaborations. So, the CMS Collaboration has measured the double differential cross section $d\sigma/dp_T dy$ in the range $18 < p_T < 196$ GeV at $\sqrt{s} = 7$ TeV in five b -jet rapidity regions, namely, $|y(b)| < 0.5$, $0.5 < |y(b)| < 1$, $1 < |y(b)| < 1.5$, $1.5 < |y(b)| < 2$ and $2 < |y(b)| < 2.2$ as a function of the leading b -jet transverse momentum [45]. In the ATLAS analysis [46], the inclusive b -jet cross section was measured

⁸The derived TMD quark densities in a proton can be tested, for example, with Dell-Yan processes, where quark distributions play a leading role. However, we leave it for the dedicated study.

⁹<https://theory.sinp.msu.ru/doku.php/pegasus/news>

as a function of transverse momentum p_T in the range $20 < p_T(b) < 400$ GeV and four rapidity subdivisions, $|y(b)| < 0.3$, $0.3 < |y(b)| < 0.8$, $0.8 < |y(b)| < 1.2$ and $1.2 < |y(b)| < 2.1$. In addition, the $b\bar{b}$ -dijet cross section was measured as a function of the dijet invariant mass M in the range $110 < M < 760$ GeV, azimuthal angle difference $\Delta\phi$ between the two leading b -jets and angular variable $\chi = \exp|y_1 - y_2|$ for jets with $p_T > 40$ GeV in two dijet mass regions, $110 < M < 370$ GeV and $370 < M < 850$ GeV.

The results of our calculations are shown in Figs. 4 and 5 in comparison with experimental data [45, 46]. Here we plot predictions based on both differential and integral KMR/WMR definitions (37) and (38) — (40) with the AO condition applied. Additionally, we show the results obtained by employing the integral formula (27), where the conventional PDFs from CT'14 set [24] have been used as an input, as it was done earlier (see Fig. 3). Solid histograms corresponds to our central results, where we fixed both renormalization and factorization scales at their default values. The shaded bands correspond to scale uncertainties of our calculations with (38) — (40). As usual, the latter were estimated by varying the scales μ_R and μ_F by a factor of 2 around their default values. We find that good agreement with the LHC data on the b -jet transverse momenta is achieved with integral KMR/WMR definition in each of the rapidity subdivisions, both in normalization and shape (green histograms). In contrast, the predictions based on the differential definition overestimate the data at central rapidities and large transverse momenta, thus leading to a worse description of the data (see Fig. 4). However, these predictions are close to the data in forward kinematical region in the whole p_T range. At low and moderate transverse momenta results obtained with both KMR/WMR definitions practically coincide. The predictions based on conventional PDFs from CT'14 set tend to underestimate the data at low $p_T \sim 20$ GeV and overestimate the data at large $p_T \sim 400$ GeV at forward rapidities. The observed difference in predictions for b -jet transverse momentum distributions is an immediate consequence of the difference between these gluon densities at large \mathbf{k}_T^2 shown in Fig. 3. So, the general conclusion [63] that integral KMR/WMR definition with ordinary PDFs used as an input is more preferable for phenomenological application is confirmed. Specially we point out a good description of the LHC data at large p_T , where the essentially large x region is probed. That is due to accurate taking into account large- x asymptotics of solutions of the DGLAP equations in our present calculations. Note that in our previous consideration [47] such extension of the TMD parton densities to the large- x region has been modelled.

Both the considered above analytical expressions (37) and (38) — (40) as well as the general formula (27) with CT'14 set results in a good (within the estimated uncertainties) description of $b\bar{b}$ -dijet cross sections reported by the ATLAS Collaboration, as it is demonstrated in Fig. 5. Such events provide us with additional observables which are a useful complementary ones. In particular, good agreement of our predictions and measured $\Delta\phi$ distributions is remarkable, where $\Delta\phi$ is the difference between the azimuthal angles of the produced b -jets. The latter is known to be strongly sensitive to the high-order pQCD corrections encoded in the \mathbf{k}_T^2 shape of the TMD parton densities (see [42, 43]). In fact, $\Delta\phi$ distribution degenerates into δ -function at $\phi = 0$ at the LO pQCD and continuous spectra can only be obtained by including higher-order corrections, which are automatically taken into account in our calculations in the form of TMD parton densities in a proton.

Another interesting observable in $b\bar{b}$ -dijet production is the angular variable χ . This variable is constructed in a way that the $2 \rightarrow 2$ cross section of elastic scattering of two point-like massless particles is approximately constant as a function of $\chi \sim (1 + \cos\theta^*)/(1 - \cos\theta^*)$, where θ^* is the scattering angle in the center-of-mass frame. It was argued [46] that this observable is relatively insensitive to the uncertainties related with

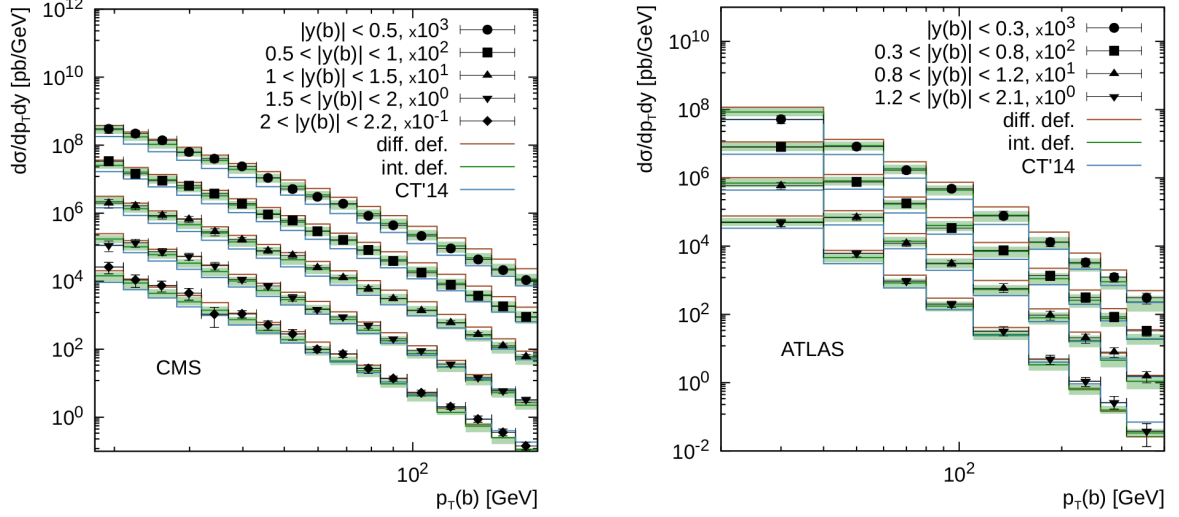


Figure 4: The transverse momentum distributions of inclusive b -jet production at $\sqrt{s} = 7$ TeV as functions of the leading jet transverse momentum in different rapidity regions. The kinematical cuts are described in the text. The experimental data are from CMS [45] and ATLAS [46].

the PDFs behaviour at small x . One can see that the χ distribution is well reproduced by our theoretical calculations based on both KMR/WMR definitions. The distribution flattens for large invariant mass M .

Finally, we conclude that the newly derived analytical expressions for the TMD parton densities in a proton, valid in the whole x range, agree well with available LHC data on heavy flavor production in pp collisions. The integral definition of the KMR/WMR approach (38) — (40) provides a better description of the data. The corresponding TMD gluon distribution in a proton, labelled as KL'2025, is already available for public usage and implemented into the TMDLIB package [69] and Monte-Carlo event generator PEGASUS [68]. It supersedes our previous KLSZ'2020 set.

5 Conclusion

We presented the analytical expressions for the Transverse Momentum Dependent parton densities in a proton. These expressions are derived at leading order of the QCD running coupling and valid at both small and large x . The calculations are performed using the Kimber-Martin-Ryskin/Watt-Martin-Ryskin approach with different treatment of kinematical constraint, which reflects the angular and strong ordering conditions for parton emissions at the last step of the QCD evolution. Both the differential and integral definitions of the KMR/WMR scenario are considered. As an input, the analytical solution of DGLAP equations for conventional parton distributions in a proton is applied, where the valence and non-singlet quark parts obey the Gross-Llewellyn-Smith and Gottfried sum rules and momentum conservation for the singlet quark and gluon densities is taken into account.

We demonstrated that the derived expressions agree well with the LHC data on inclusive heavy flavor production in pp collisions at high energies. It was confirmed that the integral definition of the KMR/WMR approach provides better description of the data and more preferable in the phenomenological applications. The corresponding TMD

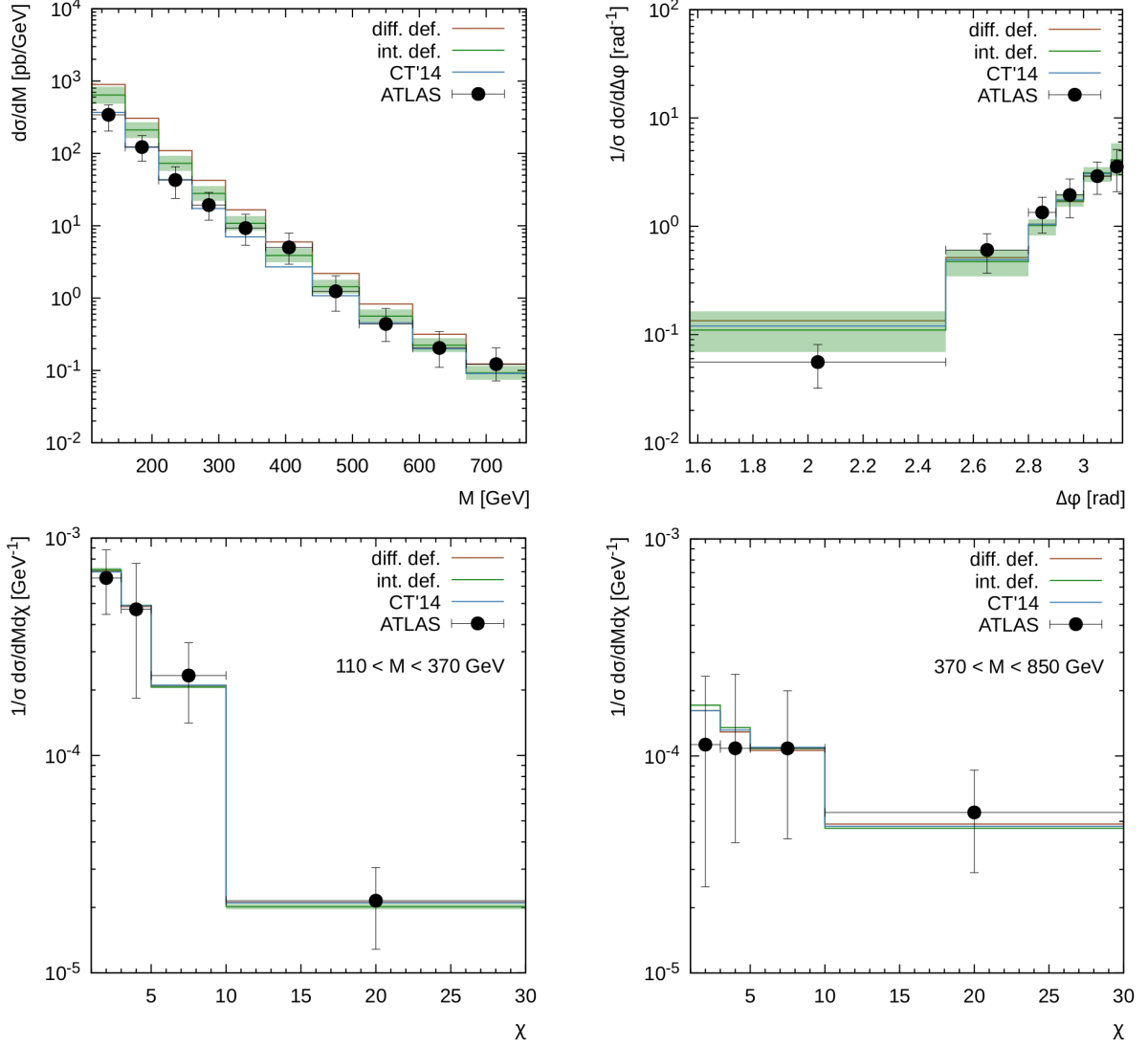


Figure 5: The $b\bar{b}$ -dijet invariant mass M , azimuthal angle difference $\Delta\phi$ and χ distributions of $b\bar{b}$ production at $\sqrt{s} = 7$ TeV. The kinematical cuts are described in the text. The experimental data are from ATLAS [46].

gluon distribution in a proton, labelled as KL'2025, is already available for public usage and implemented into the TMDLIB package and Monte-Carlo event generator PEGASUS. It supersedes our previous KLSZ'2020 set.

The main advantage of developed approach is related with quite compact analytical formulas for the TMD parton densities in a proton, which could be easily applied in further phenomenological studies. Of course, the presented LO analysis can be considered as one of the first steps in our investigations in this direction. So, we are going to improve the accuracy to the NLO level in forthcoming studies. Also, we plan to extend the consideration to nuclear PDFs and nuclear TMDs (following [49, 70]) by using the results for the whole x range presented here). It is important for future studies of proton-nucleus and nucleus-nucleus interactions within the TMD-based approaches.

Acknowledgements

We thank S.P. Baranov, M.A. Malyshev and H. Jung for their interest, very important comments and remarks. Our study was carried out at the expence of the Russian Science Foundation grant 25-2200066.

References

- [1] S. Catani, M. Ciafaloni, F. Hautmann, Nucl. Phys. B **366**, 135 (1991);
J.C. Collins, R.K. Ellis, Nucl. Phys. B **360**, 3 (1991).
- [2] L.V. Gribov, E.M. Levin, M.G. Ryskin, Phys. Rep. **100**, 1 (1983);
E.M. Levin, M.G. Ryskin, Yu.M. Shabelsky, A.G. Shuvaev, Sov. J. Nucl. Phys. **53**, 657 (1991).
- [3] J.C. Collins, D.E. Soper, Nucl. Phys. B **194**, 445 (1982).
- [4] J.C. Collins, D.E. Soper, Nucl. Phys. B **197**, 446 (1982).
- [5] J.C. Collins, D.E. Soper, G.F. Sterman, Nucl. Phys. B **223**, 381 (1983).
- [6] J.C. Collins, D.E. Soper, G.F. Sterman, Nucl. Phys. B **250**, 199 (1985).
- [7] R. Angeles-Martinez, A. Bacchetta, I.I. Balitsky, D. Boer, M. Boglione, R. Boussarie, F.A. Ceccopieri, I.O. Cherednikov, P. Connor, M.G. Echevarria, G. Ferrera, J. Grados Luyando, F. Hautmann, H. Jung, T. Kasemets, K. Kutak, J.P. Lansberg, A. Lelek, G.I. Lykasov, J.D. Madrigal Martinez, P.J. Mulders, E.R. Nocera, E. Petreska, C. Pisano, R. Placakyte, V. Radescu, M. Radici, G. Schnell, I. Scimemi, A. Signori, L. Szymanowski, S. Taheri Monfared, F.F. Van der Veken, H.J. van Haevermaet, P. Van Mechelen, A.A. Vladimirov, S. Wallon, Acta Phys. Polon. B **46**, 2501 (2015).
- [8] A.V. Lipatov, S.P. Baranov, M.A. Malyshev, Phys. Part. Nucl. **55**, 256 (2024).
- [9] E.A. Kuraev, L.N. Lipatov, V.S. Fadin, Sov. Phys. JETP **44**, 443 (1976);
E.A. Kuraev, L.N. Lipatov, V.S. Fadin, Sov. Phys. JETP **45**, 199 (1977);
I.I. Balitsky, L.N. Lipatov, Sov. J. Nucl. Phys. **28**, 822 (1978).
- [10] V.N. Gribov, L.N. Lipatov, Sov. J. Nucl. Phys. **15**, 438 (1972);
L.N. Lipatov, Sov. J. Nucl. Phys. **20**, 94 (1975);
G. Altarelli, G. Parisi, Nucl. Phys. B **126**, 298 (1977);
Yu.L. Dokshitzer, Sov. Phys. JETP **46**, 641 (1977).

- [11] M. Ciafaloni, Nucl. Phys. B **296**, 49 (1988);
S. Catani, F. Fiorani, G. Marchesini, Phys. Lett. B **234**, 339 (1990);
S. Catani, F. Fiorani, G. Marchesini, Nucl. Phys. B **336**, 18 (1990);
G. Marchesini, Nucl. Phys. B **445**, 49 (1995).
- [12] I. Balitsky, Nucl. Phys. B **463**, 99 (1996);
Y.V. Kovchegov, Phys. Rev. D **60**, 034008 (1999).
- [13] J. Jalilian-Marian, A. Kovner, A. Leonidov, H. Weigert, Phys. Rev. D **59**, 014014 (1998).
- [14] J. Jalilian-Marian, A. Kovner, A. Leonidov, H. Weigert, Phys. Rev. D **59**, 014015 (1998).
- [15] A. Kovner, J.G. Milhano, H. Weigert, Phys. Rev. D **62**, 114005 (2000).
- [16] E. Iancu, A. Leonidov, L.D. McLerran, Nucl. Phys. A **692**, 583 (2001).
- [17] H. Weigert, Nucl. Phys. A **703**, 823 (2002).
- [18] E. Ferreira, E. Iancu, A. Leonidov, L. McLerran, Nucl. Phys. A **703**, 489 (2002).
- [19] M.A. Kimber, A.D. Martin, M.G. Ryskin, Phys. Rev. D **63**, 114027 (2001).
- [20] A.D. Martin, M.G. Ryskin, G. Watt, Eur. Phys. J. C **31**, 73 (2003).
- [21] A.D. Martin, M.G. Ryskin, G. Watt, Eur. Phys. J. C **66**, 163 (2010).
- [22] NNPDF Collaboration, Eur. Phys. J. C **82**, 428 (2022).
- [23] S. Bailey, T. Cridge, L.A. Harland-Lang, A.D. Martin, R.S. Thorne, Eur. Phys. J. C **81**, 341 (2021).
- [24] S. Dulat, T.-J. Hou, J. Gao, M. Guzzi, J. Huston, P. Nadolsky, J. Pumplin, C. Schmidt, D. Stump, C.-P. Yuan, Phys. Rev. D **93**, 033006 (2016).
- [25] T.-J. Hou, T.J. Hobbs, K. Xie, S. Dulat, M. Guzzi, J. Huston, P. Nadolsky, J. Pumplin, C. Schmidt, I. Sitiwaldi, D. Stump, C.-P. Yuan, Phys. Rev. D **103**, 014013 (2021).
- [26] R. Wang, X. Chen, Chin. Phys. C **41**, 053103 (2017).
- [27] R. Maciula, R. Pasechnik, A. Szczurek, Phys. Rev. D **106**, 054018 (2022).
- [28] A. Cisek, A. Szczurek, Phys. Rev. D **103**, 114008 (2021).
- [29] K. Golec-Biernat, L. Motyka, T. Stebel, Phys. Rev. D **103**, 034013 (2021).
- [30] M. Modarres, M.R. Masouminia, R. Aminzadeh-Nik, H. Hosseinkhani, N. Olanj, Phys. Rev. D **94**, 074035 (2016).
- [31] B. Guiot, A. van Hameren, Phys. Rev. D **104**, 094038 (2021).
- [32] F.E. Barattini, C.O. Dib, B. Guiot, arXiv:2501.17662 [hep-ph].
- [33] R. Maciula, A. Szczurek, Phys. Rev. D **100**, 054001 (2019);
A.A. Chernyshev, V.A. Saleev, Phys. Rev. D **110**, 114031 (2024).

- [34] S.P. Baranov, A.V. Lipatov, A.A. Prokhorov, X. Chen, Eur. Phys. J. C **84**, 348 (2024).
- [35] N.A. Abdulov, A.V. Kotikov, A.V. Lipatov, Particles **5**, 535 (2022).
- [36] BCDMS Collaboration, Phys. Lett. B **223**, 485 (1989).
- [37] H1 Collaboration, Eur. Phys. J. C **64**, 561 (2009).
- [38] H1 Collaboration, JHEP **09**, 061 (2012).
- [39] H1 Collaboration, Eur. Phys. J. C **74**, 2814 (2014).
- [40] H1 and ZEUS Collaborations, JHEP **01**, 109 (2010).
- [41] ZEUS Collaborations, Phys. Rev. D **90**, 072002 (2014).
- [42] N.P. Zotov, A.V. Lipatov, V.A. Saleev, Phys. Atom. Nucl. **66**, 755 (2003).
- [43] H. Jung, M. Krämer, A.V. Lipatov, N.P. Zotov, JHEP **1101**, 085 (2011);
H. Jung, M. Krämer, A.V. Lipatov, N.P. Zotov, Phys. Rev. D **85**, 034035 (2012).
- [44] CMS Collaboration, Phys. Lett. B **772**, 306 (2017).
- [45] CMS Collaboration, JHEP **1204**, 084 (2012).
- [46] ATLAS Collaboration, Eur. Phys. J. C **71**, 1846 (2011).
- [47] A.V. Kotikov, A.V. Lipatov, B.G. Shaikhatdenov, P.M. Zhang, JHEP **02**, 028 (2020).
- [48] A.V. Kotikov, A.V. Lipatov, P.M. Zhang, Phys. Rev. D **104**, 054042 (2021).
- [49] A.V. Lipatov, M.A. Malyshev, A.V. Kotikov, X. Chen, Phys. Lett. B **850**, 138486 (2024).
- [50] A.V. Kotikov, V.G. Krivokhizhin, Phys. Atom. Nucl. **68**, 1873 (2005);
A.V. Kotikov, V.G. Krivokhizhin, Phys. Part. Nucl. **40**, 1059 (2009).
- [51] A.V. Kotikov, V.G. Krivokhizhin, B.G. Shaikhatdenov, Phys. Rev. D **81**, 034008 (2010);
A.V. Kotikov, B.G. Shaikhatdenov, N.S. Korchagin, P. Zhang , arXiv:2403.13360 [hep-ph].
- [52] A.Yu. Illarionov, A.V. Kotikov, S.S. Parzycki, D.V. Peshekhonov, Phys. Rev. D **83**, 034014 (2011).
- [53] C. Lopez, F.J. Yndurain, Nucl. Phys. B **171**, 231 (1980);
C. Lopez, F.J. Yndurain, Nucl. Phys. B **183**, 157 (1981).
- [54] A.V. Kotikov, A.V. Lipatov, N.P. Zotov, JETP **101**, 811 (2005).
- [55] G. Cvetič, A.Yu. Illarionov, B.A. Kniehl, A.V. Kotikov, Phys. Lett. B **679**, 350 (2009).
- [56] A.V. Kotikov, V.N. Velizhanin, arXiv:hep-ph/0501274.
- [57] NM Collaboration, Nucl. Phys. B **483**, 3 (1997);
S. Kumano, Phys. Rept. **303**, 183 (1998).

- [58] A.V. Kotikov, B.G. Shaikhatdenov, P.M. Zhang, Phys. Rev. D **96**, 114002 (2017).
- [59] A.V. Kotikov, G. Parente, Nucl. Phys. B **549**, 242 (1999).
- [60] A.Yu. Illarionov, A.V. Kotikov, G. Parente, Phys. Part. Nucl. **39**, 307 (2008).
- [61] A.V. Kotikov, B.G. Shaikhatdenov, Phys. Part. Nucl. **48**, 829 (2017);
A.V. Kotikov, B.G. Shaikhatdenov, Phys. Atom. Nucl. **78**, 525 (2015);
A.V. Kotikov, B.G. Shaikhatdenov, Phys. Part. Nucl. **44**, 543 (2013).
- [62] L. Mankiewicz, A. Saalfeld, T. Weigl, Phys. Lett. B **393**, 175 (1997).
- [63] K. Golec-Biernat, A.M. Stasto, Phys. Lett. B **781**, 633 (2018).
- [64] B. Guiot, Phys. Rev. D **101**, 054006 (2020).
- [65] R.K. Valeshabadi, M. Modarres, Eur. Phys. J. C **82**, 66 (2022).
- [66] B. Guiot, Phys. Rev. D **107**, 014015 (2023).
- [67] Particle Data Group Collaboration, Phys. Rev. D **110**, 030001 (2024).
- [68] A.V. Lipatov, M.A. Malyshev, S.P. Baranov, Eur. Phys. J. C **80**, 330 (2020).
- [69] N.A. Abdulov, A. Bacchetta, S.P. Baranov, A. Bermudez Martinez, V. Bertone, C. Bissolotti, V. Candelise, L.I. Estevez Banos, M. Bury, P.L.S. Connor, L. Favart, F. Guzman, F. Hautmann, M. Hentschinski, H. Jung, L. Keersmaekers, A.V. Kotikov, A. Kusina, K. Kutak, A. Lelek, J. Lidrych, A.V. Lipatov, G.I. Lykasov, M.A. Malyshev, M. Mendizabal, S. Prestel, S. Sadeghi Barzani, S. Sapeta, M. Schmitz, A. Signori, G. Sorrentino, S. Taheri Monfared, A. van Hameren, A.M. van Kampen, M. Vanden Bemden, A. Vladimirov, Q. Wang, H. Yang, Eur. Phys. J. C **81**, 752 (2021).
- [70] N.A. Abdulov, A.V. Kotikov, A.V. Lipatov, Phys. Part. Nucl. Lett. **20**, 557 (2023);
N.A. Abdulov, X. Chen, A.V. Kotikov, A.V. Lipatov, JETP Lett. **118**, 723 (2023);
A.V. Kotikov, A.V. Lipatov, P.M. Zhang, JETP Lett. **119**, 745 (2024).